A System for the Aerodynamic Optimization of Three-Dimensional Configurations

M. Orlowski, W. Tang

Institute of Design Aerodynamics, German Aerospace Center (DLR)
Lilienthalplatz 7, D-38108 Braunschweig, Germany

Summary

The paper presents a system for the aerodynamic optimization of three-dimensional configurations. This system is based on the repeated calculation of the flowfield around three-dimensional geometries by solving the Euler/Navier-Stokes equations. The basic structure of the system and the incoperated modules are described. Under the same conditions the system must provide the same solutions of classic aerodynamic optimization problems as given in literature. So the function of the system is checked with the Rhombus airfoil and the Sears-Haack body. The potential of the system is demonstrated with current aerodynamic optimization problems.

List of Symbols

A	area
C_D	drag coefficient
C_L	lift coefficient
c	chord length
D	drag
d	diameter
d_{CB}	diameter of capsule base
F_{CS}	area of capsule surface
G	objective function
L	lift
l	length
l_{REF}	reference length (= 10 m)
M	Mach number
r_{CN}	radius of capsule nose
S	parameter
$\overline{S}$	parameter set
$\Delta\overline{S}$	stepsize
U	volume utility ($= V/F^{3/2}$)
V	volume
α	angle of attack
δ	maximum thickness

Indices

B	body
C	capsule
SSB	SCT body
SSC	SCT cone
SSW	SCT wing
∞	freestream

1 Introduction

Future military and civilian aerospace vehicles must fulfil extensive and partially conflicting requirements. Technical aspects like flying characteristics or stealth capabilities have to be considered as well as economical aspects like life-cycle costs or fleet compatibilities and ecological aspects like noxious emissions or noise regulations. In order to fulfil these requirements the close interaction of all involved disciplines and the optimal use of all technical potentialities is necessary. Simultaneously, design cycle times have to be reduced.

Size and complexity of this task lead to growing importance of numerical design and optimization methods. In general, these methods can be divided based on their orientation into multidisciplinary methods and disciplinary methods. Multidisciplinary methods are used mainly in the predesign stage for a rough assessment of the vehicle characteristics and a preliminary interaction of the involved disciplines. An overview of multidisciplinary design and optimization methods is given in Ref. 1. Disciplinary methods are used mainly in the design stage for an exact calculation of the vehicle characteristics and their improvement. An overview of disciplinary design and optimization methods is given in Ref. 2.

Most aerodynamic design and optimization methods are still based on linear theory. They cannot or cannot exactly model nonlinear phenomenons like separations or vortices. Hence, results represent only approximations of real optima. In order to improve these approximations the Institute of Design Aerodynamics of the German Aerospace Center (DLR) is working on new methods[3-5] based on non-linear theory, i.e. the solution of the Euler/Navier-Stokes equations.

Section 2 deals with the fundamentals of such an aerodynamic optimization method. The basic structure of the computational system and the incoporated modules are described. Tests of the system make up section 3. Its function is checked with solutions of classic aerodynamic optimization problems: the Rhombus airfoil and the Sears-Haack body. Section 4 presents applications of the system. Aerodynamic optimizations of a biconic re-entry capsule, an SCT wing as well as an SCT wing/body configuration and their results are presented.

2 Aerodynamic Optimization System

The Aerodynamic Optimization System is based on the repeated calculation of flowfields around three-dimensional geometries. A mathematical algorithm gives changes of the respective geometry according to an optimization strategy. These changes are carried out, the spatial mesh is created and the flowfield computed. The changes are characterized by the resulting aerodynamic coefficients and judged with an objective function. Finally, the mathematical algorithm determines the changes of the respective

Paper presented at the RTO AVT Symposium on "Aerodynamic Design and Optimisation of Flight Vehicles in a Concurrent Multi-Disciplinary Environment", held in Ottawa, Canada, 18-21 October 1999, and published in RTO MP-35.

geometry, which fulfil the demands formulated through the objective function best.

2.1 Basic Structure

The basic structure of the Aerodynamic Optimization System and the course of events is depicted in Fig. 1. Input parameters are start values for the geometric and aerodynamic parameters, which are included in the optimization process, constraints limiting their variations, start values for the stepsizes, which are used to determine gradients, and the objective function. These parameters have influence in the whole system. Further input parameters are values for the geometric and aerodynamic parameters, which are not included in the optimization process, and instructions for the generation of the surface mesh, the generation of the spatial mesh and the calculation of the flowfield. These parameters have influence only in certain modules.

At the beginning a geometry corresponding to the geometric parameters and a surface mesh are created. For that the instructions for the generation of the surface mesh prescribe the number of points in axial and spanwise direction, the location of points near edges and corners, the distribution of points near shocks and separations etc. Based on the surface mesh a spatial mesh is created. The instructions for the generation of the spatial mesh prescribe the number of points normal to the surface, the location of the farfield, the distribution of points etc.

Then the flowfield around the geometry is computed and the aerodynamic coefficients are determined. A numerical method is used to solve the Euler/Navier-Stokes equations at every point of the spatial mesh. The instructions for the calculation of the flowfield control this method. They give the number of iteration cycles, the damping of the method etc.

In the end the aerodynamic coefficients are put into the objective function and the function is analyzed. A decision on the continuation of the optimization process is made. In case the gradients of the objective function do indicate the possibility of improvements the process is continued. The parameters, which are included in the optimization process, are changed by a mathematical algorithm according to an optimization strategy. The constraints are checked and if necessary corrections are carried out. The described steps start again, i.e. a geometry corresponding to the changed geometric parameters is generated etc. In case the gradients of the objective function do not indicate the possibility of improvements, even after changes of the stepsizes, which are used to determine the gradients, the process is stopped. The geometric parameters and the aerodynamic coefficients are stored.

So the aerodynamic optimization system is a repeated cycle of four steps: geometry generation, mesh generation, flowfield calculation and optimization. These steps are carried out within the system by four independent modules. Their communication is completely based on data files. Here advantages regarding easy maintenance and development predominate disadvantages regarding higher computational effort. The four modules are described in the following sections.

2.2 Geometry Generator

The module for the geometry generation creates, as mentioned in section 2.1, a geometry corresponding to the geometric parameters and a surface mesh. The number of parameters, which are included in the optimization process, effects directly the number of optimization cycles and so the computational effort. Hence, the module for the geometry generation should be able to define a huge variety of configurations and extensive variations of these configurations with a minimum of geometric parameters. The available CAD systems as well as *MegaCads*, the module for the mesh generation, cannot guarantee this. Because of this a new code, *MegaGeo*, has been developed and integrated.

MegaGeo composes three-dimensional configurations out of two-dimensional curves describing elements of the configurations. Figure 2 illustrates two-dimensional curves describing an airfoil. Points at the leading and trailing edge divide the airfoil into upper and lower side. Further points divide upper and lower side into segments. The number and position of these points depend on the complexity of the airfoil and the expected flexibility of the parameterization. The order of the segments determines start and end points. A set of curve functions introduced by H. Sobieczky[6] is used to define the curve in the segments. In principle all functions are controlled by four parameters, which can be associated with the slope and curvature at the start and end points. But some functions have given parameters because of their mathematical background or constraints. The key number determing upper or lower side, the coordinates of the start point, the key number determing the curve function and the parameters of the function are the necessary information for a segment.

MegaGeo distinguishes two major elements of three-dimensional configurations: Wing and body. The elements forming a wing are shown in Fig. 3. A certain number of airfoils, the leading edge, the trailing edge and the twist axis, all defined by curve functions, together with information about the transition between the airfoils and their twist build up the basic structure. All airfoils are given in a normalized way and the leading and trailing edge are used to determine their magnitude. The elements forming a body are shown in Fig. 4. A certain number of body sections, the water line and the body axis, all defined by curve functions, together with information about the transition between the sections build up the basic structure. All body sections are given in a normalized way and the water line is used to determine their magnitude.

The surface of a wing, a body or a wing/body configuration develops with the surface mesh. For that a distribution of planes $x = const.$ is given. In these planes the intersection between wing and body results from a calculation. Also in these planes the number of mesh points as well as their distribution on wing and body, defined by curve functions too, is given. So the complete geometry and surface mesh generation is based on parameters controlling curve functions and can be carried out as an automatic generation. The instructions for the generation of the geometry and the surface mesh are more or less equivalent to these parameters.

2.3 Mesh Generator

The module for the mesh generation creates, as mentioned in section 2.1, a spatial mesh based on the surface mesh created by the module for the geometry generation. It has to guarantee an automatic generation of high quality within the optimization process. A huge variety of configurations and extensive variations of these configurations should not call this into question. Furthermore, it has to guarantee an automatic generation with minimum computational effort. The DLR code *MegaCads*[7] fulfils this and has been integrated.

MegaCads enables the definition of structured multi-block meshes around complex three-dimensional configurations using a parametric approach. Basic techniques for the generation of ge-

ometries and different algorithms for the determination of surface/surface intersections are integrated. Efficient algebraic methods for two and three-dimensional mesh generation are available. In order to smooth the algebraic meshes elliptic algorithms can be used allowing different controls for the point distribution at boundaries. Support features for multi-grid and chimera techniques are developed. The complete interactive mesh generation is stored in a protocol file using a simple script language and can be repeated for similar configurations or within an optimization process as an automatic generation. The instructions for the generation of the spatial mesh are more or less equivalent to this protocol file.

2.4 Flow Solver

The module for the flowfield calculation computes, as mentioned in section 2.1, the flowfield around the geometry and determines the aerodynamic coefficients. The flowfield calculation solving the Euler/Navier-Stokes equations has by far the greatest share of the computational effort. Hence, the module should be able to carry out one calculation with minimum computational effort as well as high robustness and accuracy. The DLR code *CEVCATS* and its successor *FLOWer*[8] fulfil this and have been integrated.

CEVCATS and *FLOWer* solve the Euler/Navier-Stokes equations using a second-order accurate finite-volume method. The spatial discretization is done by means of a cell-vertex scheme and central differences. In order to damp numerical oscillations first and second-order dissipative terms are added to the governing equations according to A. Jameson[9]. The integration in time of the resulting system of ordinary differential equations is carried out by means of an explicit five-stage Runge-Kutta scheme. To accelerate convergence local time stepping, residual smoothing and multi-grid algorithms are used. The instructions for the calculation of the flowfield are more or less equivalent to the input file of *CEVCTAS* or *FLOWer.*

2.5 Optimization Algorithm

The module for the optimization analyses, as mentioned in section 2.1, the objective function, makes a decision on the continuation of the optimization process, changes the parameters and checks the constraints. It has to guarantee a certain determination of global extreme. Complex structures of the parameter space or numerical fluctuations of the objective function should not call this into question. Furthermore, it has to guarantee a determination with minimum computational effort. The algorithm *EXTREM* developed by H.G. Jakob[10] fulfils this and has been integrated.

EXTREM determines the changes of the geometry, which fulfil the demands formulated through the objective function best, applying finite differences and parabolic interpolation. Figure 5 sketches the principle of the optimization strategy and the function of the mathematical algorithm. The start point of the optimization process, the parameter set $\overline{S}_0$, and the primary search direction $\Delta\overline{S}$ are given as input data. Search steps $\overline{S}_1 = \overline{S}_0 - \Delta\overline{S}$ and $\overline{S}_2 = \overline{S}_0 + \Delta\overline{S}$ lead to the parameter sets $\overline{S}_1$ and $\overline{S}_2$. Values of the objective function at the parameter sets $\overline{S}_0$, $\overline{S}_1$ and $\overline{S}_2$ are used for the assessment of the extreme in the primary search direction by means of parabolic extrapolation. The parameter set $\overline{S}_3$ results. At $\overline{S}_3$ a secondary search direction perpendicular to the primary direction is defined with an orthogonalization procedure. Further search steps lead to the parameter sets $\overline{S}_4$ and $\overline{S}_5$. The assessment of the extreme in secondary search direction by means of parabolic extrapolation leads to the parameter set $\overline{S}_6$. For a parameter space created by n parameters (n-1) secondary search directions are defined. Hence, for a parameter space created by 2 parameters a so called step is completed with the parameter set $\overline{S}_6$. After such a step a new primary search direction passing through the last parameter set and the last parameter set of the previous step (or the start point) is defined. The described procedure starts again, i.e. search steps lead to new parameter sets etc. It continues until the gradients of the objective function do not indicate the possibility of improvements, even after changes of the step-sizes.

EXTREM considers constraints of the parameters, which limit the variations, depending on the occurring violation. In case the violation of a constraint is caused by a search step, the step is neglected and the new parameter set results from a step with half of the previous size in the opposite direction. In case the violation of a constraint is caused by a parabolic extrapolation, the step is also neglected and the new parameter set results from a step with a quarter of the calculated size in the search direction. Of course EXTREM checks the constraints with the new parameter sets as well and carries out again necessary corrections in the same way.

3 Test of the Optimization System

Several solutions of classic aerodynamic optimization problems are documented in literature, solutions based on linear theory, extended linear theory or exact theory. Under the same conditions the aerodynamic optimization system must provide these solutions as well. Even under different conditions regarding the flowfield calculation the system must provide similar solutions. This has been checked with two classic aerodynamic optimization problems.

3.1 Rhombus Airfoil

The first problem is the symmetric airfoil of given length and thickness, which has minimum drag in supersonic flow. Linear theory[11] results in an airfoil with straight flanks before and behind the maximum thickness, a so-called rhombus airfoil. The maximum thickness of this airfoil lies at $x/c = 0.5$, i.e. exactly at half chord length. It depends not on the Mach number. The drag coefficient amounts to $C_D = 0.00208$ for Mach number $M_\infty = 2.0$ and $C_D = 0.00321$ for Mach number $M_\infty = 1.5$ assuming a relative thickness of $\delta/c = 0.03$. Extended linear and exact theory[12] result also in an airfoil with straight flanks before and behind the maximum thickness. But the maximum thickness lies not exactly at half chord length. It depends on the Mach number and lies at $x/c = 0.5191$ for Mach number $M_\infty = 2.0$ and at $x/c = 0.5192$ for Mach number $M_\infty = 1.5$, i.e. behind half chord length. The maximum thickness moves closer to the trailing edge with increasing Mach number. The drag coefficient amounts to $C_D = 0.00205$ for Mach number $M_\infty = 2.0$ and $C_D = 0.00317$ for Mach number $M_\infty = 1.5$ assuming a relative thickness of $\delta/c = 0.03$.

Several optimizations of a symmetric airfoil with respect to minimum drag in supersonic flow and based on solutions of the Euler equations have been carried out. They included five geometric parameters sketched in Fig. 6: the position of the maximum thickness in x-direction, the slope of the flank before the maximum thickness at the leading edge and at the maximum thickness as well as the slope of the flank behind the maximum thickness at the maximum thickness and at the trailing edge. Figures 7 and 8

depict initial and resulting airfoils for Mach number $M_\infty = 2.0$ using different start values for the parameters and stepsizes. All optimizations lead to the same airfoil. Hence, the resulting airfoil is not a coincidence. An effect of the start values could not be found. The optimizations lead to an airfoil agreeing very good with the solution based on extended linear and exact theory. The maximum thickness lies at $x/c = 0.5157$ compared to $x/c = 0.5192$ based on extended linear and exact theory. Difference between both values is about 1%. The drag coefficient amounts to $C_D = 0.00209$ compared to $C_D = 0.00205$ based on extended linear and exact theory. Difference is about 2%.

Figure 9 depicts initial and resulting airfoils for Mach number $M_\infty = 1.5$ Again, the optimization leads to an airfoil agreeing very good with the solution based on extended linear and exact theory. The maximum thickness lies at $x/c = 0.5162$ compared to $x/c = 0.5192$ based on extended linear and exact theory. Difference between both values is about 0.5%. The drag coefficient amounts to $C_D = 0.00322$ compared to $C_D = 0.00317$ based on extended linear and exact theory. Difference is 2%.

Besides the effect of start values for the parameters and stepsizes the effect of accuracy as well as mesh density has been investigated. As mentioned in section 2.1, a numerical method is used to solve the Euler/Navier-Stokes equations at every point of the spatial mesh and to determine the aerodynamic coefficients. The accuracy, where this method stops, can be varied. Resulting airfoils for Mach number $M_\infty = 2.0$ determing the aerodynamic coefficients with different accuracies are shown in Fig. 10. Up to 10^{-4} an effect of the accuracy cannot be found. Figure 11 plots the computational effort on a NEC SX4 for the optimizations with different accuracies. Here an effect can be found. In accordance to expectations lower accuracies lead to lower computational effort. A spatial mesh is necessary solve the Euler equations and to determine the aerodynamic coefficients. The number of mesh points can be varied. Resulting airfoils for Mach number $M_\infty = 2.0$ using spatial meshes of different densities are shown in Fig. 12. Up to 1275 points only a small effect of the density can be found. Figure 13 plots the computational effort for the optimizations with different mesh densities. Again, in accordance to expectations lower densities lead to lower computational effort.

3.2 Sears-Haack Body

The second classic aerodynamic optimization problem is the body of revolution of given length and volume, which has minimum drag in supersonic flow. Linear theory[13] results in body with the maximum thickness at $x/l_B = 0.5$, i.e. exactly at half body length. The position depends not on the Mach number. The drag coefficient amounts to $C_D = 0.1104$ for Mach number $M_\infty = 2.0$ as well as for Mach number $M_\infty = 1.5$ assuming a volume of $V_B/l^3_{REF} = 0.0046$. The coefficient depends also not on the Mach number. Extended linear theory[14] results in a body with the maximum thickness not at half body length. The position depends on the Mach number and lies at $x/l_B = 0.5107$ for Mach number $M_\infty = 2.0$ and at $x/l_B = 0.5110$ for Mach number $M_\infty = 1.5$, i.e. behind half body length. It moves closer to the tail with increasing Mach number. A drag coefficient cannot be calculated.

Several optimizations of a body of revolution with respect to minimum drag in supersonic flow and based on solutions of the Euler equations have been carried out. They included six geometric parameters sketched in Fig. 14: the position of the maximum thickness in x- and z-direction, the slope of the contour at the nose, before the maximum thickness, behind the maximum thickness and at the tail. Some of these parameters are given because of constraints. The contour has to be continual at the maximum thickness. Hence, the slope of the contour before and behind the maximum thickness must be equal, i.e. zero. The volume has to be constant. Therefore, the slope at the tail must be chosen depending on the position of the maximum thickness and the slope at the nose. Figures 15 and 16 depict initial and resulting bodies for Mach number $M_\infty = 2.0$ using different start values for the parameters and stepsizes. All optimizations lead to the same body. Hence, the resulting body is not a coincidence. An effect of the start values cannot be found. The optimizations lead to a body agreeing very good with the solution based on extended linear theory. The maximum thickness lies at $x/l_B = 0.5028$ compared to $x/l_B = 0.5107$ based on extended linear theory. Difference between both values is about 1.5%. The drag coefficient amounts to $C_D = 0.0889$.

Figure 17 depicts initial and resulting bodies for Mach number $M_\infty = 1.5$. Again, the optimization leads to a body agreeing very good with the solution based on extended linear theory. The maximum thickness lies at $x/l_B = 0.4942$ compared to $x/l_B = 0.5110$ based on extended linear theory. Difference between both values is about 3%. The drag coefficient amounts to $C_D = 0.0949$.

Resulting bodies for Mach number $M_\infty = 2.0$ determing the aerodynamic coefficients with different accuracies are shown in Fig. 18. Up to 10^{-4} an effect of the accuracy cannot be found. Figure 19 plots the computational effort on a NEC SX4 for the optimizations with different accuracies. Here an effect can be found. In accordance to expectations lower accuracies lead to lower computational effort. Resulting bodies for Mach number $M_\infty = 2.0$ using spatial meshes of different densities are shown in Fig. 20. Up to 14985 points only a small effect of the density can be found. Figure 21 plots the computational effort for the optimizations with different mesh densities. Again, in accordance to expectations lower densities lead to lower computational effort.

So the aerodynamic optimization system provides the same solutions for classic aerodynamic optimization problems as given in literature. Input parameters, accuracy of the flowfield calculation and density of the spatial mesh have no effect on the solution. But they have a significant effect on the computational effort.

4 Application of the Optimization System

Different kinds of aerodynamic optimization problems are encountered during the design of aerospace vehicles. With several examples the potential of the Aerodynamic Optimization System has been proven. Three examples are documented in the following sections.

4.1 Re-entry Capsule

The aerodynamic characteristics of re-entry vehicles are very important for their mission. They decide the time frame of the re-entry, the place for the landing, the strain on the crew as well as the necessity for reactive or aerodynamic control systems. Hence, an improvement of the characteristics increases the possibilities for the mission and occasionally the financial requirements.

Several optimizations of a biconic re-entry capsule with respect to various objective functions and based on solutions of the Euler

equations have been carried out. The included seven geometric parameters are sketched in Fig. 22: the radius of the nose, the angles of the first and second cone, the length of the first and second cone, the inclination angle of the first cone and the diameter of the base. Some of these parameters are given because of constraints, which have been taken into account for a realistic background. The radius of the nose has to be larger than $r_{CN}/l_{REF} = 0.02$ in order to guarantee reasonable heat loads. The diameter of the base has to be $d_{CB}/l_{REF} = 0.35$ for good structural contact with launch systems. Finally, the volume of the capsule has to be $V_C/l^3_{REF} = 0.03$ in oder to accommodate crew, systems etc. Hence, the length of the second cone must be chosen depending on the angles of the first and second cone and the length of the first cone.

Figure 23 depicts resulting capsules for Mach number $M_\infty = 6.0$ with and without taking the stability into account. The objective function is identical. Taking the stability not into account leads to a long and slender capsule. A difference between the first and second cone angle cannot be found. Taking the stability into account by moving the center of gravity leads to a shorter capsule. A difference between the first an second cone angle can be found. Lift-to-drag ratios depending on the angle of attack are plotted in Fig. 24. Taking the stability not into account causes significantly higher lift-to-drag ratios.

Figure 25 depicts resulting capsules for Mach number $M_\infty = 6.0$ using different objective functions. The stability is taken into account. High weighting on the lift-to-drag ratio leads to a long and slender capsule again. High weighting on the volume efficiency leads to a shorter capsule. As expected high weighting on the lift-to-drag ratio causes higher lift-to-drag ratios, see Fig. 26. In this case bending of the capsule by an inclination angle of the first cone increases the ratios even more. In the other case, high weighting on the volume efficiency, bending provides no benefit.

Figure 27 depicts resulting capsules for Mach number $M_\infty = 6.0$ and Mach number $M_\infty = 1.5$. The objective function is identical, the stability is taken into account. For Mach number $M_\infty = 1.5$ the resulting capsule has a greater radius of the nose. Its lift-to-drag ratios are lower, see Fig. 28.

4.2 SCT Wing

The aerodynamic characteristics of the wing are crucial for an aircraft. The wing produces by far the greatest share of the drag. Hence, an improvement of the characteristics decreases the fuel consumption and by this way increases the economic efficiency of the aircraft.

Several optimizations of the wing for a Supersonic Commercial Transport with respect to minimum drag at cruise conditions and based on solutions of the Euler equations have been carried out. They included 31 geometric parameters. The parameters concerning the planform of the wing are sketched in Fig. 29: the position of the points at the wing tip in x-direction and in x- as well as y-direction, the position of the points at the leading-edge kink and the trailing-edge kink in x- as well as y-direction and the position of the point at the trailing edge root in x-direction. All points are connected with straight lines. The parameters concerning the airfoils at the root, at half of the half-span and at the tip are similar to those in Fig. 6: the position of the maximum thickness in x-direction, the slope of the flank before the maximum thickness at the leading edge and at the maximum thickness, the slope of the flank behind the maximum thickness at the maximum thickness and at the trailing edge, the shift of the airfoils in z-direction, the chamber and the local angle of attack. Some of these parameters are given because of constraints, which have been taken into account for a realistic background. The area of the wing has to be $A_{SSW}/l^2_{REF} = 4.5$. Hence, the position of the trailing edge must be chosen depending on the span of the wing as well as the position of the leading-edge kink and the trailing-edge kink. The contour has to be continual at the maximum thickness of the airfoils. As a result the slop of the flanks before and behind the maximum thickness must be equal, i.e. zero. The volume of the wing has to be $V_{SSW}/l^3_{REF} = 0.0167$ and the maximum thickness of the airfoils has to be $\delta/c = 0.025$. Therefore, the slopes at the trailing edge must be chosen depending on the positions of the maximum thickness and the slopes at the leading edge. Furthermore, the lift coefficient of the wing has to be $C_L = 0.12$ at Mach number $M_\infty = 2.0$. This is ensured by the objective function.

Figure 30 depicts the initial and the resulting wing of one optimization. The resulting wing has a greater span than the initial wing. In order to keep the area its length is smaller. The resulting wing has a nearly straight leading edge. The kink has vanished. Figure 31 depicts the initial and the resulting airfoils in a normalized way. Chamber, local angle of attack etc. are very small and have been neglected here. The resulting airfoils are similar. They have a position of the maximum thickness slightly before half chord length. The lift-to-drag ratio of the resulting wing amounts at $M_\infty = 2.0$ to $L/D = 16$.

4.3 SCT Wing/Body Configuration

Several optimizations of an SCT wing/body configuration with respect to minimum drag at cruise conditions and based on solutions of the Euler equations have also been carried out. The included nine geometric parameters are sketched in Fig. 32: the length and diameter of the cylindrical body part, the length and diameter of the nose and tail cone, the position of the wing in x- and z-direction and the inclination angle of the body. Nose and tail cone have been shaped like Sears-Haack bodies, the wing has been taken from Ref. 15 and kept constant. Some of the parameters are given because of constraints, which have been taken into account for a realistic background. The body has to accommodate 250 passengers at 6 seats per row. Hence, according to guidelines the body must have a diameter of $d_{SSB}/l_{REF} = 0.35$ for 6 seats per row and based on this a length of $l_{SSB}/l_{REF} = 5.71$ for 250 passengers. The contour has to be continual at the transition from the nose cone to the cylindrical body part and from the cylindrical body part to the tail cone. Therefore, the nose and tail cone must have a diameter of $d_{SSC}/l_{REF} = 0.35$. Similar to the optimization of the SCT wing the lift coefficient of the configuration has to be $C_L = 0.1$ at Mach number $M_\infty = 2.0$ and angle of attack $\alpha = 3°$. This is ensured by the objective function. An assessment of viscous drag by the flat plate analogy is included in the objective function.

Fig. 33 depicts the initial and the resulting configurationof an optimization. The resulting configuration has a significantly greater length of the nose and tail cone than the initial configuration. It has a position of the wing closer to the nose and a greater inclination angle of the body. Lift-to-drag ratios depending on the angle of attack are plotted in Fig. 34. The resulting configuration has significantly higher lift-to-drag ratios than the initial configuration, not only in the design point, i.e. at angle of attack $\alpha = 3°$, but also at other angles of attack.

5 Conclusions

The described Aerodynamic Optimization System has proven to be a useful tool for the aerodynamic optimization of three-dimensional configurations. The system is based on the repeated calculation of the flowfield around three-dimensional geometries by solving the Euler/Navier-Stokes equations. Hence, non-linear phenomenons influence the optima. Under the same conditions the system has provided the same solutions of classic aerodynamic optimization problems as given in literature. Input parameters, accuracy of the flowfield calculation and density of the spatial mesh had in a reasonable range no effect on the solutions. But they had a significant effect on the computational effort. The Aerodynamic Optimization System has shown its potential for current aerodynamic optimization problems. Improvements of a re-entry capsule, an SCT wing and an SCT wing/body configuration before a realistic background have been achieved.

References

1 Sobieszczanski-Sobieski, J. and Haftka, R.T., *"Multidisciplinary Aerospace Design Optimization: Survey of Recent Developments"*, AIAA 96-0711.

2 Foster N.F. et al., *"Three-Dimensional Aerodynamic Shape Optimization Using Genetic Evolution and Gradient Search Algorithms"*, AIAA 96-0555.

3 Strohmeyer, D. and Seubert, R., *"Improvement of a Preliminary Design and Optimization Program for the Evaluation of Future Aircraft Projects"*, AIAA 98-4828.

4 Orlowski, M. and Herrmann, U., *"Aerodynamic Optimization of Supersonic Transport Configurations"*, ICAS 96-4.3.3.

5 Bartelheimer, W., *"An Improved Integral Equation Method for the Design of Transonic Airfoils and Wings"*, AIAA 95-1688.

6 Sobieczky, H., *"Geometry Generation for Transonic Design"*, In: Recent Advances in Numerical Methods in Fluids Vol. 4 (Ed. Habashi, W.G.), Pineridge Press, Swansea, 1985, pp. 163-182.

7 Brodersen, O. et al., *"The Parametric Grid Generation System MegaCads"*, In: Proc. 5th International Conference on Numerical Grid Generation in Computational Field Simulations (Eds. Soni, B.K., Thompson, J.F., Häuser, J., Eisemann, P.R.), Mississippi, 1996, pp. 353-362.

8 Kroll, N. et al., *"Accurate and Efficient Flow Solvers for 3D Applications on Structured Meshes"*, VKI Lecture Series 94-05 on Computational Fluid Dynamics, Brussels, 1994.

9 Jameson, A. et al., *"Numerical Solution of the Euler-Equations by Finite Volume Methods using Runge-Kutta Time-Stepping Schemes"*, AIAA 81-1259.

10 Jakob, H.G., *"Rechnergestützte Optimierung statischer und dynamischer Systeme - Beispiele mit FORTRAN Programmen"*, Fachberichte Messen, Steuern und Regeln Vol. 6, Springer Verlag, Berlin, 1982.

11 Miele, A. *"Theory of Optimum Aerodynamic Shapes"*, Academic Press, New York, 1965.

12 Ferri, A. *"Elements of Aerodynamics of Supersonic Flows"*, Macmillan Company, New York, 1949.

13 Sears, W.R., *"On Projectiles of Minimum Wave Drag"*, Quarterly Applied Mathematics Vol. 14 (1947), pp. 361-366.

14 Wellmann, J., *"Der Einfluß der Machzahl auf wellenwiderstandsoptimierte Rümpfe und Profile bei Überschallanströmung"*, DLR Report 151-73/5 (1973).

15 Doherty, J.J. and Parker, N.T., *"Dual-Point Design of a Supersonic Transport Wing Using a Constrained Optimization Method"*, In: Proc. 7th European Aerospace Conference, Toulouse, 1994, pp. 247-265.

Figures

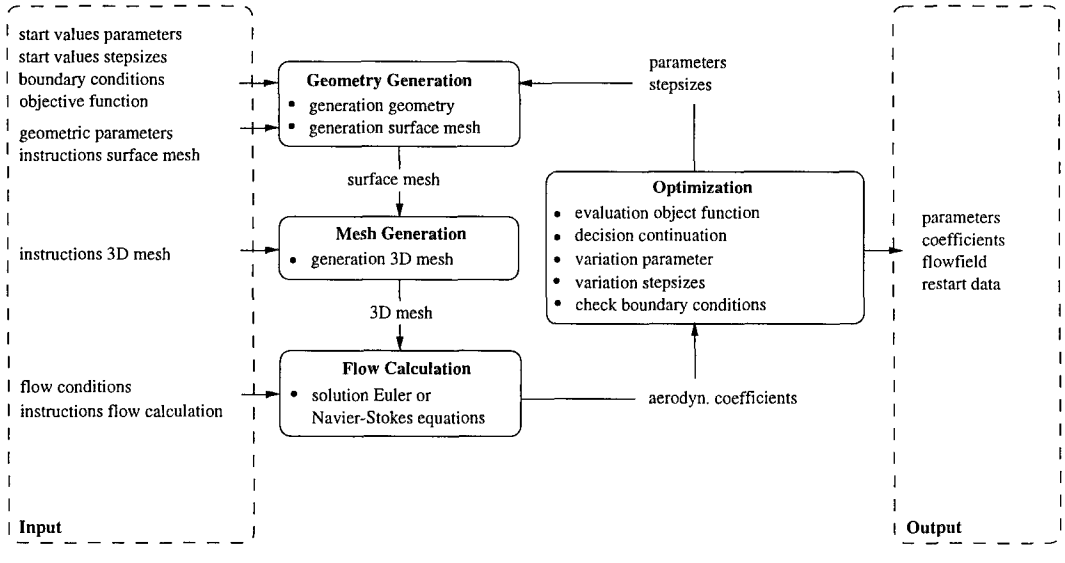

Figure 1: Basic structure of the Aerodynamic Optimization System.

Sketch:

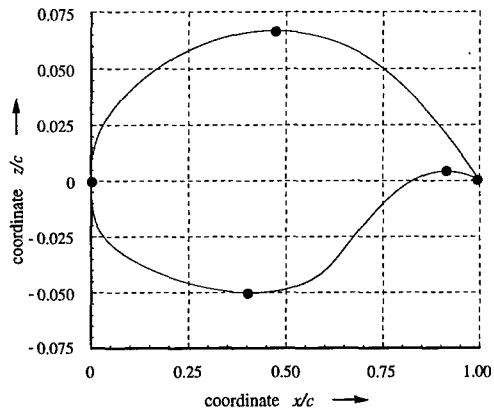

Data:

key number upper/lower side	coordinate x/c start point	coordinate z/c start point	slope start point	key number curve function	slope end point	curvature start point	curvature end point
1	0.000	0.000		7	0.0	6.0	4.0
1	0.475	0.065	0.0	1	-0.2	4.0	2.0
1	1.000	0.000					
2	0.000	0.000		7	0.0	6.0	4.5
2	0.400	-0.050	0.0	1	0.0	4.5	8.0
2	0.920	0.005	0.0	1	-0.1	8.0	2.0
2	1.000	0.000					

Figure 2: Example for curve functions describing an airfoil.

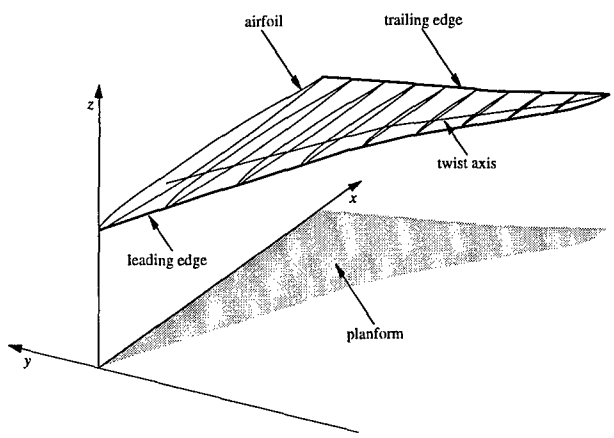

Figure 3: Elements forming a wing.

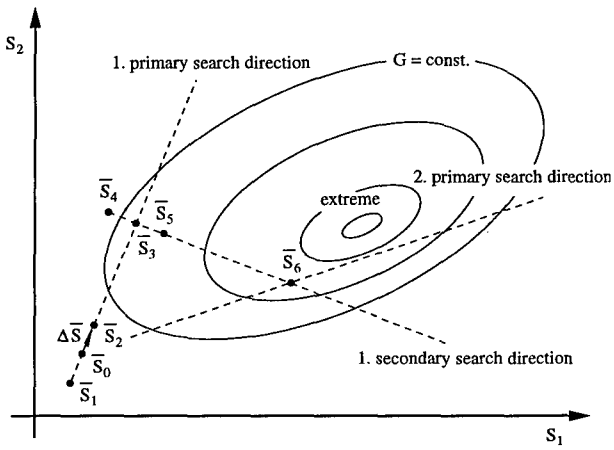

Figure 5: Principle function of the optimization algorithm.

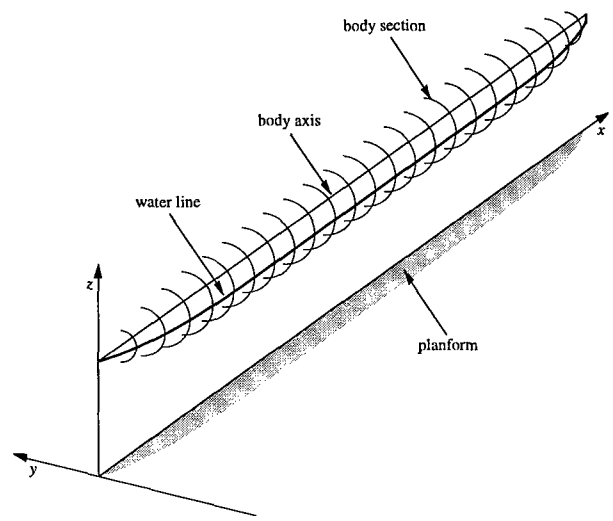

Figure 4: Elements forming a body.

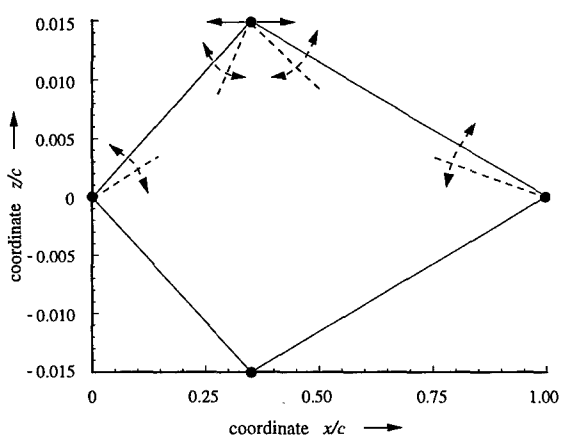

Figure 6: Symmetric airfoil with 5 geometric parameters, maximum thickness $\delta/c = 0.03$.

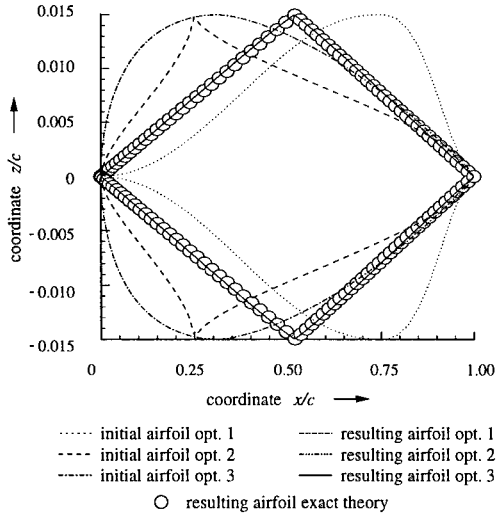

Figure 7: Initial and resulting airfoils of optimizations at Mach number $M_\infty = 2.0$ using different start values for the parameters.

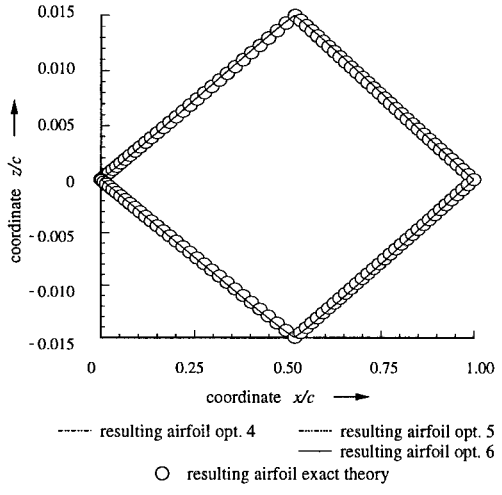

Figure 8: Resulting airfoils of optimizations at Mach number $M_\infty = 2.0$ using different start values for the stepsizes.

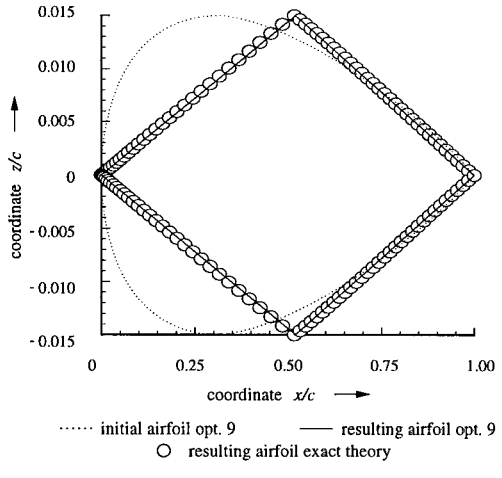

Figure 9: Initial and resulting airfoils of an optimizations at Mach number $M_\infty = 1.5$.

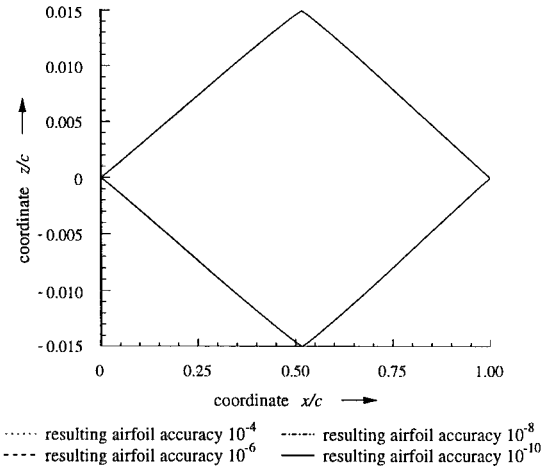

Figure 10: Resulting airfoils of optimizations at Mach number $M_\infty = 2.0$ determing the aerodynamic coefficients with different accuracies.

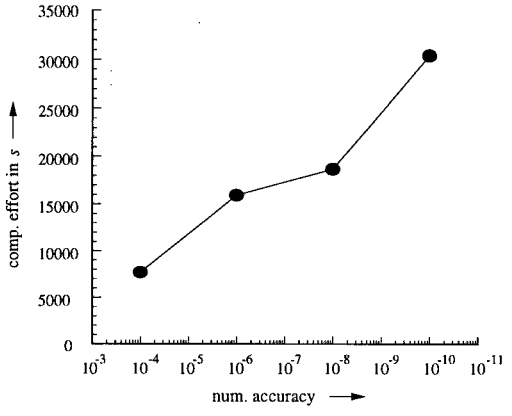

Figure 11: Computational effort for the optimizations at Mach number $M_\infty = 2.0$ determing the aerodynamic coefficients with different accuracies.

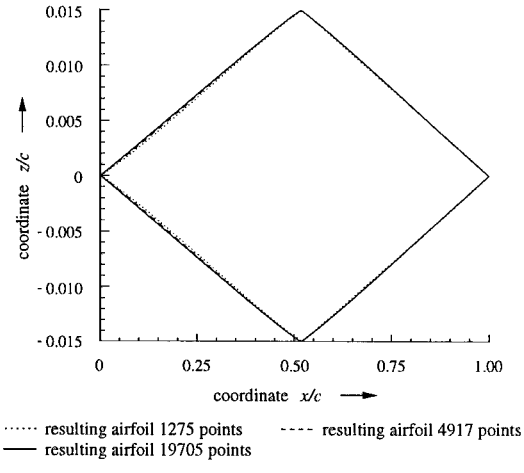

Figure 12: Resulting airfoils of optimizations at Mach number $M_\infty = 2.0$ using spatial meshes of different densities.

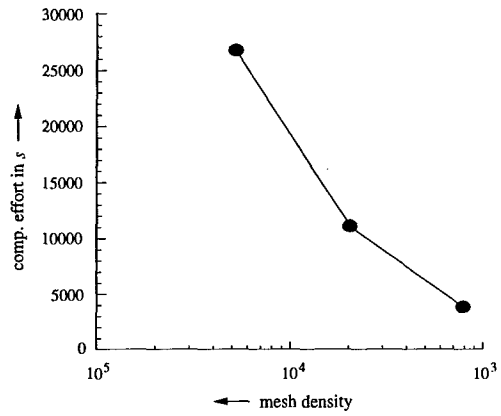

Figure 13: Computational effort for the optimizations at Mach number $M_\infty = 2.0$ using spatial meshes of different densities.

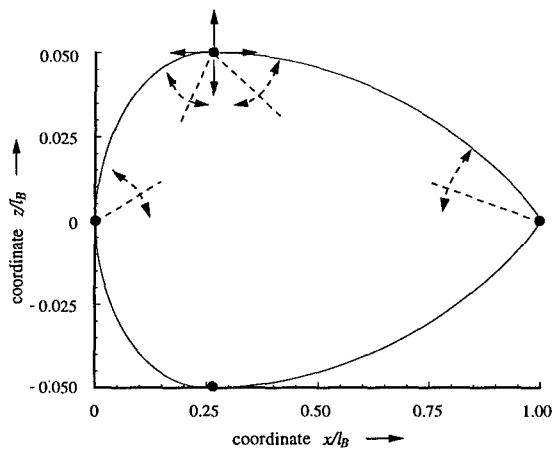

Figure 14: Body of revolution with 6 geometric parameters, volume $V_B/l^3_{REF} = 0.0046$.

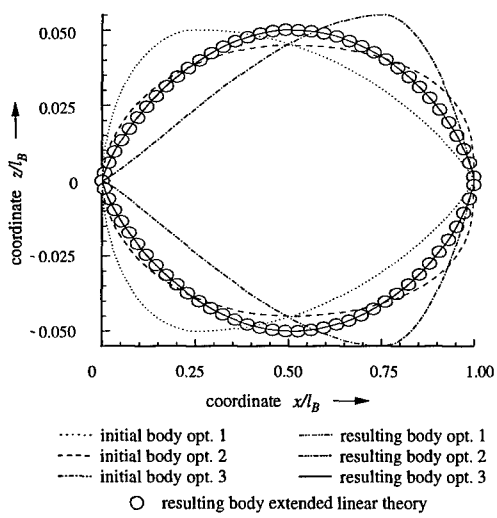

Figure 15: Initial and resulting bodies of optimizations at Mach number $M_\infty = 2.0$ using different start values for the parameters.

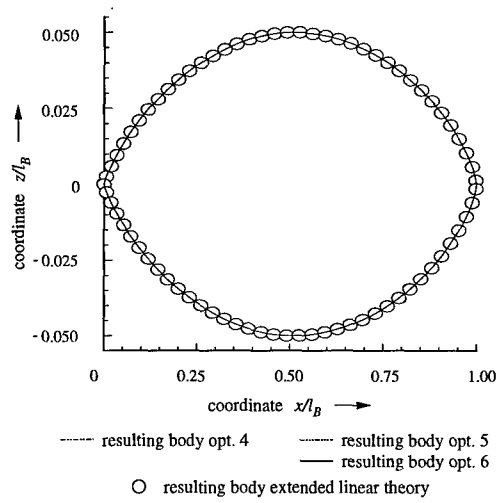

Figure 16: Resulting bodies of optimizations at Mach number $M_\infty = 2.0$ using different start values for the stepsizes.

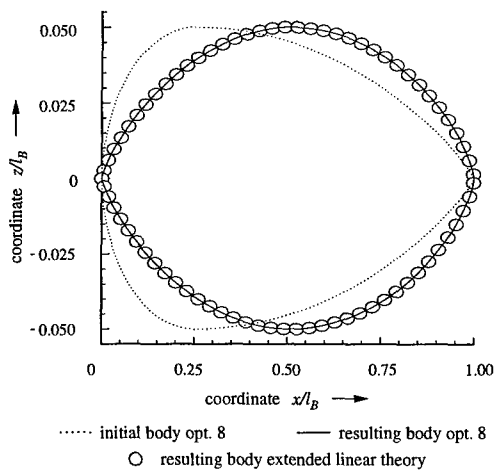

Figure 17: Initial and resulting body of an optimization at Mach number $M_\infty = 1.5$.

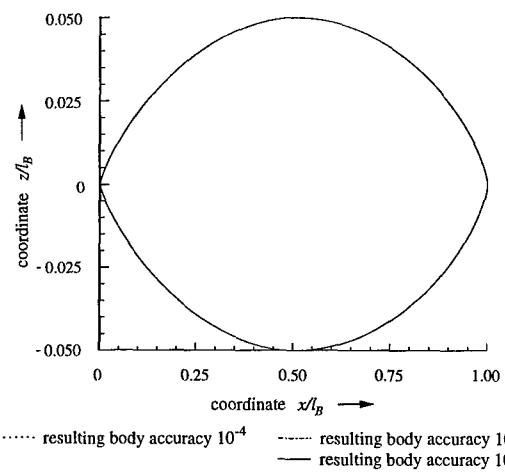

Figure 18: Resulting bodies of optimizations at Mach number $M_\infty = 2.0$ determing the aerodynamic coefficients with different accuracies.

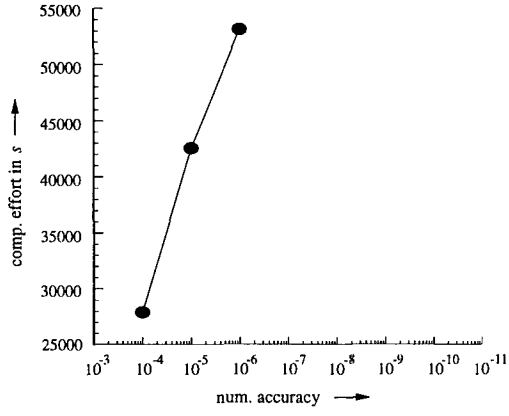

Figure 19: Computational effort for the optimizations at Mach number $M_\infty = 2.0$ determing the aerodynamic coefficients with different accuracies.

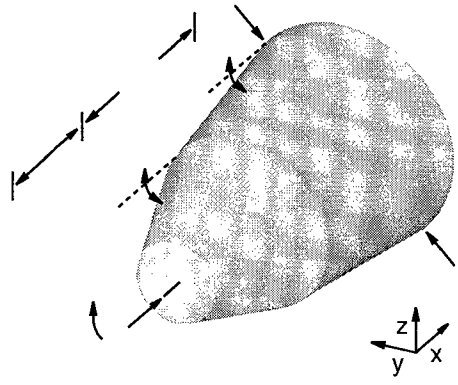

Figure 22: Biconic re-entry capsule with 7 geometric parameters, volume $V_C/l^3_{REF} = 0.03$, base diameter $d_{CB}/l_{REF} = 0.35$.

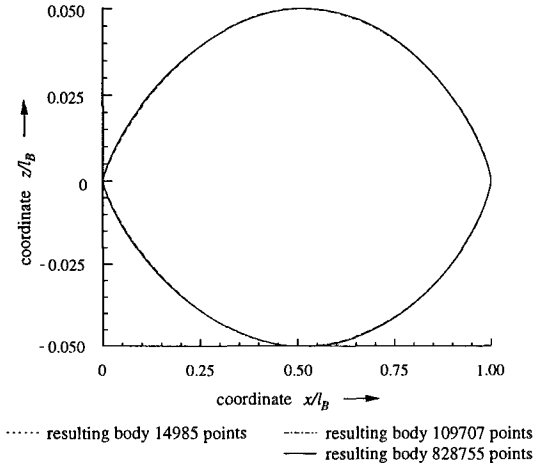

Figure 20: Resulting bodies of optimizations at Mach number $M_\infty = 2.0$ using spatial meshes of different densities.

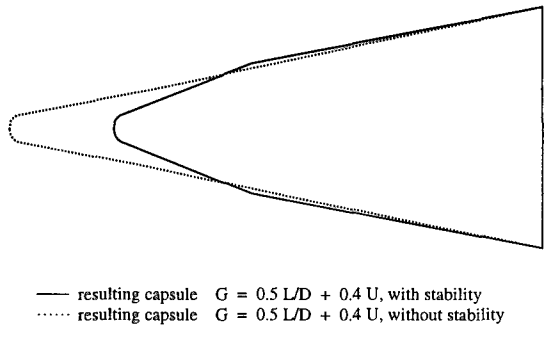

Figure 23: Resulting biconic re-entry capsules of optimizations at Mach number $M_\infty = 6.0$ with and without taking the stability into account.

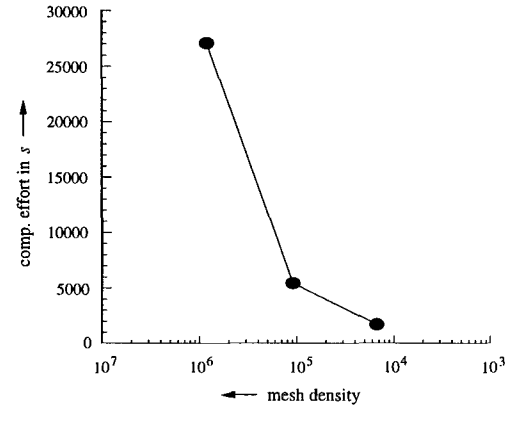

Figure 21: Computational effort for the optimizations at Mach number $M_\infty = 2.0$ using spatial meshes of different densities.

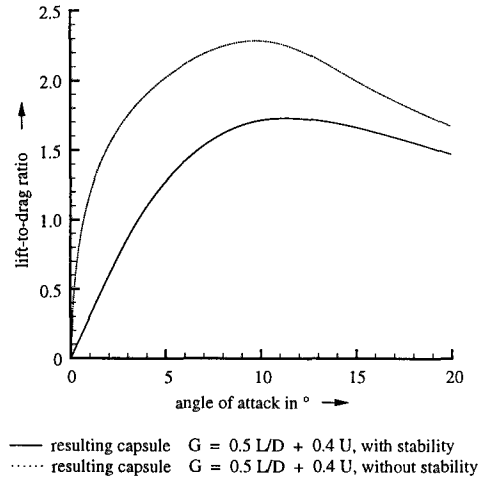

Figure 24: Lift-to-drag ratios of the biconic re-entry capsules resulting from optimizations at Mach number $M_\infty = 6.0$ with and without taking the stability into account.

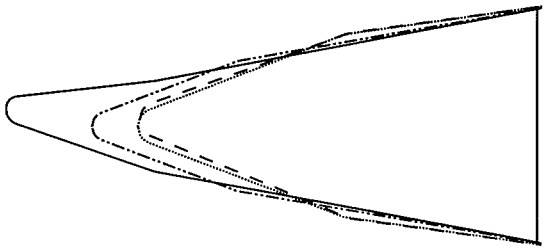

resulting capsule G = 0.7 L/D + 0.2 U
resulting capsule G = 0.7 L/D + 0.2 U, bent
resulting capsule G = 0.2 L/D + 0.9 U
resulting capsule G = 0.2 L/D + 0.9 U, bent

Figure 25: Resulting biconic re-entry capsules of optimizations at Mach number $M_\infty = 6.0$ with different objective functions.

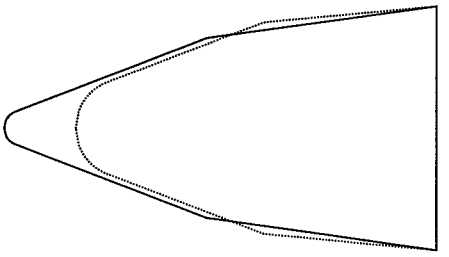

resulting capsule G = 0.2 L/D + 0.9 U, M = 6.0
resulting capsule G = 0.2 L/D + 0.9 U, M = 1.5

Figure 27: Resulting biconic re-entry capsules of optimizations at Mach number $M_\infty = 6.0$ and at Mach number $M_\infty = 1.5$.

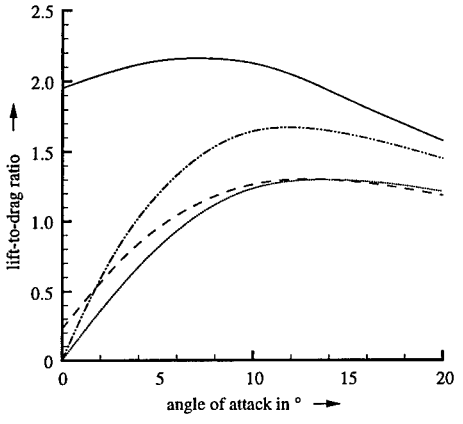

resulting capsule G = 0.7 L/D + 0.2 U
resulting capsule G = 0.7 L/D + 0.2 U, bent
resulting capsule G = 0.2 L/D + 0.9 U
resulting capsule G = 0.2 L/D + 0.9 U, bent

Figure 26: Lift-to-drag ratios of the biconic re-entry capsules resulting from optimizations at Mach number $M_\infty = 6.0$ with different objective functions.

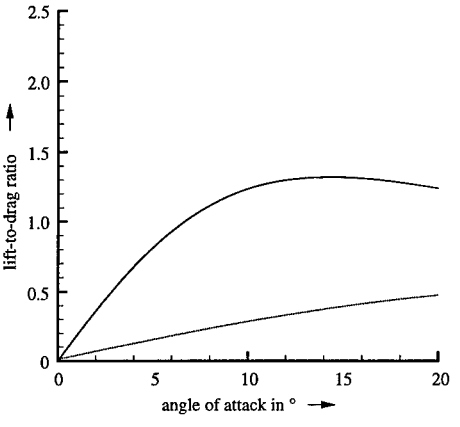

resulting capsule G = 0.2 L/D + 0.9 U, M = 6.0
resulting capsule G = 0.2 L/D + 0.9 U, M = 1.5

Figure 28: Lift-to-drag ratios of the biconic re-entry capsules resulting from optimizations at Mach number $M_\infty = 6.0$ and at Mach number $M_\infty = 1.5$.

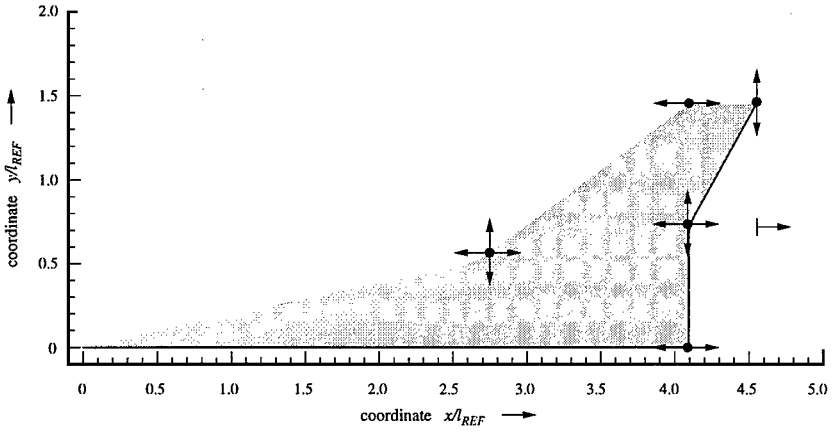

Figure 29: Planform of the wing for a Supersonic Commercial Transport with 8 parameters, volume $V_{SSW}/l^3_{REF} = 0.0167$, area $A_{SSW}/l^2_{REF} = 4.5$ and lift coefficient $C_L = 0.12$.

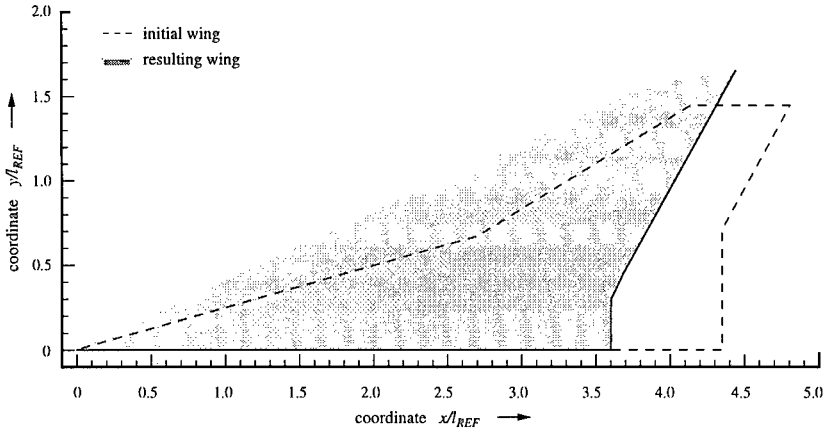

Figure 30: Planform of the initial and resulting SCT wing of an optimization at Mach number $M_\infty = 2.0$.

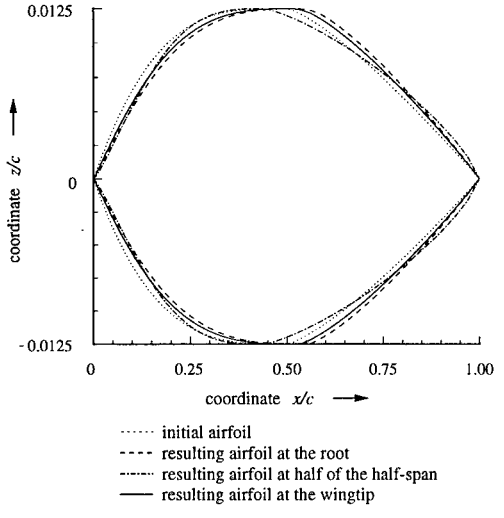

Figure 31: Normalized airfoils of the initial and resulting SCT wing of an optimization at Mach number $M_\infty = 2.0$.

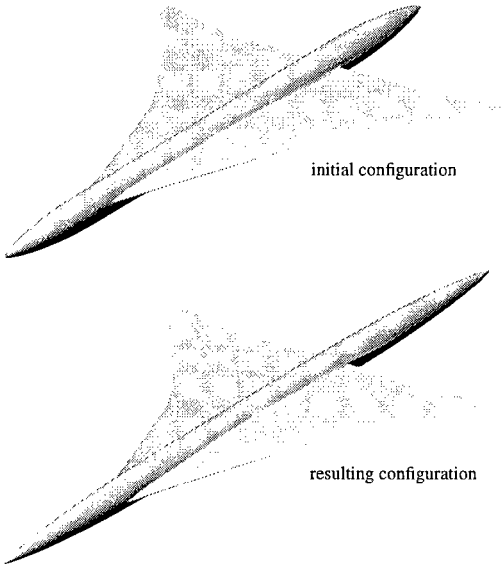

Figure 33: Initial and resulting SCT wing/body configurations resulting from an optimization at Mach number $M_\infty = 2.0$ and angle of attack $\alpha = 3°$.

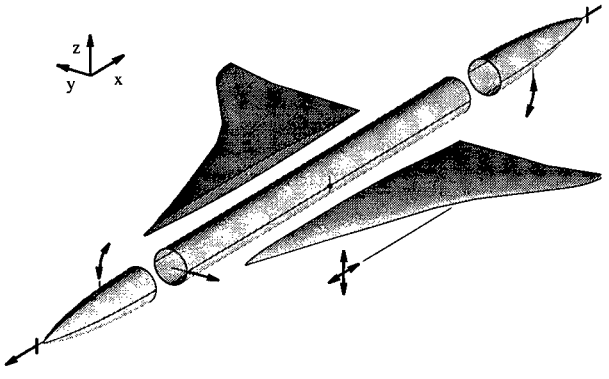

Figure 32: Wing/body configuration for a Supersonic Commercial Transport with 9 parameters, 250 passengers in 6 seats per row, wing fixed and lift coefficient $C_L = 0.1$.

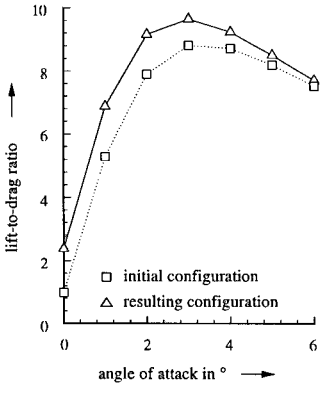

Figure 34: Lift-to-drag ratios of the initial and resulting SCT wing/body configuration resulting from an optimization at Mach number $M_\infty = 2.0$ and angle of attack $\alpha = 3°$.

DISCUSSION

Session III, Paper #19

Prof Knight (Rutgers University, USA) asked the largest number of design variables the author had considered. He wanted to know how the author's approach would "scale up" to problems involving large numbers of design variables.

> **Mr Orlowski** replied that the largest number of variables had been 35 optimizing an SCT wing. He noted that his approach using Euler equations was not cheap in terms of computational effort. He believed that with available high speed computing and experience with the system its use was acceptable, at least for the moment. He felt that further developments in computer systems available to industry should make the system acceptable to them also.

Mr Doherty (DERA, UK) asked whether it could be confirmed that the use of finite difference gradient generation rendered computation time independent of the number of constraints, unlike in an adjoint approach for gradient calculation.

> **Mr Orlowski** replied that the constraints affect the computational effort by reducing the number of parameters that are really included in the optimization process. However, the process itself was independent of this effect.